PHYSICAL REVIEW A VOLUME 24, NUMBER 5 NOVEMBER 1981

Collision spectroscopy of ion-diatom systems: He^+-N_2 and -O_2 at medium energies

D. Dowek, D. Dhuicq, J. Pommier, Vu Ngoc Tuan, V. Sidis,* and M. Barat

Laboratoire des Collisions Atomiques et Moléculaires, Bâiment 351, Université Paris-Sud, 91405 Orsay Cedex, France

(Received 23 January 1981)

Energy-loss measurements of direct-excitation and electron-capture processes are performed for the He^+-N_2, -O_2 collisional systems in the 0.2–4-keV energy range and in the 0°–3° angular range. Pure vibrational excitation and vibrational excitation in excited electronic states are studied using a high-resolution spectrometer (100 meV). Pure vibrational excitation is always found to be a weak process. The analysis of vibrational distributions in excited states strongly supports an interpretation in terms of the Franck-Condon principle. Relative probabilities as functions of energy and angle are reported for the identified excitation and electron-capture processes. The results show the importance of electron-capture processes among which quasiresonant and endothermic processes dominate exothermic processes. The striking resemblance of the present data with those available on the He^+–rare-gas systems conveys a similar quasimolecular interpretation of the collision mechanisms.

I. INTRODUCTION

The understanding of collision processes involving two atomic partners, in the medium-energy range, has considerably evolved during the past two decades. The harmonious development of both experiment and theory has enabled the field of collision spectroscopy[1] to reach maturity. On the experimental side, collision spectroscopy has consisted of measuring doubly differential cross sections (in collision energy and scattering angle) using the energy-loss technique. These data were complemented by information provided by independent total cross-section measurements of charge exchange, emission of radiation, and ejection of electrons. On the theoretical side the building up of the quasimolecular model has provided the key step of a comprehensive understanding of the collision mechanisms. These mechanisms could subsequently be investigated quantitatively owing to the rapid progress of computational technology. In contrast, the situation looks very different for ion-(atom)-molecule collisions. Indeed, the largest variety of processes (i.e., rotational, vibrational, and electronic excitation) requires a higher resolution to reach unambiguous assignments of the structures in the energy-loss spectra. Furthermore, the extension of a quasimolecular theoretical approach requires *a priori*, for the simplest atom-diatom collision, consideration of a dynamical treatment involving several triatomic energy surfaces. Except for a few attempts dealing with ion-pair formation, for which some success has been obtained with simple models,[2] the theoretical treatment of ion-molecule collisions in the moderate-energy range has remained in its infancy.

Except when stated otherwise, we will be considering atom-diatom collisions in the keV energy range (i.e., collision velocities in the range $0.01 \text{ a.u.} \lesssim v \lesssim 0.5 \text{ a.u.}$). Within this energy range one might expect that all degrees of freedom of the three nuclei do not have the same importance. It is therefore worthwhile to compare the collision time T_c with the characteristic times associated with the rotation T_r and vibration T_v of the diatomic target molecule. In the considered velocity range typical collision times range between 10^{-14} and 10^{-16} s. These figures compared with the characteristic rotation time of N_2 or O_2 ($T_r \approx 10^{-11}$ s) suggest that the molecule does not rotate *during* the collision time. On the other hand, the characteristic vibration time of N_2 or O_2 ($T_v \approx 10^{-14}$ s) may be of the same order of magnitude as the collision time. Vibration of the molecule during the collision time will then have to be considered for each system investigated.

Let us first consider pure vibrational excitation of the molecular electronic ground state. This process has been extensively investigated, as a function of scattering angle, at lower energies (few eV $\lesssim E \lesssim$ few tens of eV)[3] than considered herein. These studies have demonstrated that pure vibrational excitation occurs with a high probability at such energies, for example, the $v=0 \rightarrow 1$ transition probability reaches 50% in the H^+-H_2 collision at $E=10$ eV c.m. However, no such studies have been reported on the He^+-N_2, -O_2 systems of present interest. In the medium-energy range, resolved energy-loss spectra (ELS) for pure vibrational excitation of the ground state has only been reported for *forward* scattering.[4] These measurements have enabled the determination of total cross sections σ_{ov} for pure vibrational excitation. Typical values of the σ_{0_1} cross section lie within the range 10^{-17} to 10^{-16} cm^2.[4(b),4(c)] As a common feature of these data all σ_{0_1} cross sections reach a flat maximum for $T_c \approx T_v$. Unfortunately, this kind of measurement does not provide the *relative probability* of pure vibrational

excitation with respect to elastic scattering, since the primary beam overlaps the elastically scattered beam.

Another aspect of the investigation of the ground-state rovibrational excitation is provided by energy-loss measurements as a *function of scattering angle*.[5] In view of the limited energy resolution of the previous experiments only the mean energy loss [also called most probable energy loss (MPEL)] of the quasielastic peak (average of elastic scattering and rovibrational excitation) could be investigated. The MPEL is found to increase as a function of the reduced scattering angle $\tau = E\theta$ from a lower limit referred to as "elastic scattering" to an upper limit called "binary scattering". A number of these experiments were triggered by the classical analysis of the collision in terms of the scattering by the whole molecule (elastic scattering) or by one of the atoms constituting the molecule (binary model).[6] These concepts have later been refined[7] in order to account for the transition between these two limits as a function of τ. From the available data on the presently investigated systems there is no conclusive evidence as to whether pure vibrational and/or rotational excitation is an important process. One of the purposes of the present work (Sec. III A 1) is to investigate this problem by performing high-resolution ELS.

Let us next consider electronic excitation comprising direct and electron-capture processes. One way of investigating such processes is to study the light emitted by the excited particles.[8] Although this technique is restricted to radiating states and suffers from cascade effects, it is possible to easily identify the excited states and to test whether vibrational population agrees with the Franck-Condon (FC) prediction. It was in particular concluded by Leventhal *et al.*[8(a)] that if a collision does not transfer any vibrational energy to the molecular electronic ground state the vibrational population of an electronically excited state should follow an FC model. However, as was the case for pure vibrational excitation much new information can be gained from ELS measurements. High-resolution ELS measurements in the forward direction performed by Moore and Doering[9] on a variety of ion-diatom collisions have brought forth evidence of the excitation of specific electronic states and in some favorable cases the authors were able to resolve vibrational levels. In particular, for the He^+-N_2 collision at 2.9 keV, Moore[9(b)] states that "the relative intensity of the first six vibrational components of this ($a\,^1\Pi_g$) transition agrees to within a few percent with theoretical predictions based on calculated FC factors." On the other hand, for selected *non-zero scattering angles* no vibrationally resolved spectra for electronically excited states have, to our knowledge, been reported. The available data[10] showed significant electronic excitation of the target or projectile and sometimes (as in the recent work of Gillen)[11] allowed identification of particular electronic states. However, the most striking finding of these works for a broad variety of systems is the common behavior of the MPELs as a function of τ. The MPEL curve $Q^*(\tau)$ for each electronic excitation process is always parallel to that associated with the quasielastic process $[Q^0(\tau)]$[5,12]:

$$Q^*(\tau) \simeq Q_0(\tau) + \Delta Q\,, \tag{1}$$

where ΔQ is the electronic excitation energy in the FC region (vertical transition). This finding suggests[5(c),5(d)] that *electronic excitation occurs independently of rovibrational excitation.* This idea meets with the commonly admitted separation of electronic and nuclear motions. Although the nuclear motion may be handled using classical trajectories on multidimensional potential-energy surfaces, collisions in the medium-energy range allow an additional simplification when the comparison $T_c < T_v$ and T_R holds, namely, neglect of the variations of the diatomic internuclear vector ($\vec{r}$) (sudden approximation). With this starting point, the various pieces of information reviewed above can be reconciled in the following framework.

A certain amount of translational momentum and energy is transferred to the *nuclei of the molecule* (recoil or internal energy). Since this impulsive (shake-on-type) process lasts less than T_c, the molecule still does not rotate nor vibrate. Consequently, most electronic transitions will occur for a fixed r: *vertical transitions*. When the collision is ended the wave packet representing the internal nuclear motion of the molecule merely projects onto the final vibrorotational eigenstates associated with the ground or the excited electronic state.[13] Two cases can then be distinguished:

(a) When energy transferred to the nuclei is absorbed *exclusively as recoil* the initial vibrorotational wave packet remains *unchanged* throughout the collision. Subsequently, the energy-loss spectra should not display any rovibrational structure in the quasielastic peak. In excited electronic channels projection of the initial *unperturbed* wave packet onto the actual vibrational states yields the usual FC distribution. Case (a) which can be calcalled *extended elastic approximation*[4] should hold for very small scattering angle, especially when the impact parameter is much larger than r.

(b) When energy is also transferred to the *internal degrees of freedom* of the nuclei in the mol-

ecule the initial vibrorotational wave packet is perturbed. Here rovibrational excitation occurs in the diatom electronic ground state and the distribution of this excitation is obtained after projection of the *perturbed wave packet* onto the relevant final rovibrational eigenstates. The available data for quasielastic peaks show the envelope of this distribution centered about the MPEL. The rovibrational distribution in excited electronic states is obtained in the same way, which means that FC overlap factors should actually be calculated with the *perturbed initial rovibrational* state. Case (b) which can be called *extended pseudoelastic approximation* should hold for large scattering angle[15] especially when the impact parameter gets smaller than r. We recall that this approximation has been considered in some detail within the classical framework by Baudon[7(a)] and Sigmund[7(b),7(c)] for the case when no electronic excitation occurs.

According to the above discussion, if an electronic excitation process results from a curve-crossing mechanism, the closer in the curve crossing the larger the deviation from FC vibrorotational distribution (*stricto sensu*). It is not surprising that total cross-section measurements (which lose the information on impact parameter) may show such deviations from FC distributions.[16] On the other hand, if total cross sections for electronic excitation are very large (few to several 10^{-15} cm^2),[17] the major contributions come from impact parameters much larger than r. It can then be predicted that such a case should follow the extended elastic approximation and obey usual FC distributions.

In this paper we report detailed energy-loss measurements and excitation probabilities for the He^+-N_2, $-O_2$ collisions in the 0.2–4-keV energy range. The favorable mass ratio between the projectiles and targets allows a satisfactory resolution of various processes. Direct channels are investigated with a new spectrometer (Sec. II) intended to resolve individual vibrational levels. The additional information on electron-capture channels required to complete an overall view of the collision processes is obtained by time-of-flight (TOF) measurements. For each system (N_2, see Sec. III, O_2, see Sec. IV) the various processes are identified by their characteristic energy losses and their relative probability is then studied as a function of scattering angle. A point of the discussion (Sec V) deals with pure vibrational excitation and the relevance of the FC principle. However, the body of the interpretation treats the collision mechanisms in terms of the quasimolecular model resting on the similarities with the previously investigated He^+–rare-gas (RG) systems.[18]

II. EXPERIMENTAL TECHNIQUE

The energy-loss technique is used to investigate the two main inelastic collision processes: direct excitation of the diatomic molecule M_2 (energy loss of the scattered He^+ ions) and charge-exchange processes (energy loss of the neutralized He atoms). For this purpose two different experimental setups are used.

A. Direct-excitation processes: $He^+(1s^2S)+M_2(X)\rightarrow He^+(1s^2S)+M_2^*$

The experimental setup is shown in Fig. 1. The ion beam extracted from a discharge ion source (discharge current $I_d \simeq 100$ mA, anode voltage $V_a \simeq 90$ V) is focused, mass analyzed by a Wien filter, and decelerated before entering a double hemispherical electrostatic energy selector. The mean radius of the selector is $r = 50$ mm and the slit widths are, respectively, $f_2 = 0.4$, $f_3 = 0.4$, $S_4^{(\text{hole})}\phi$

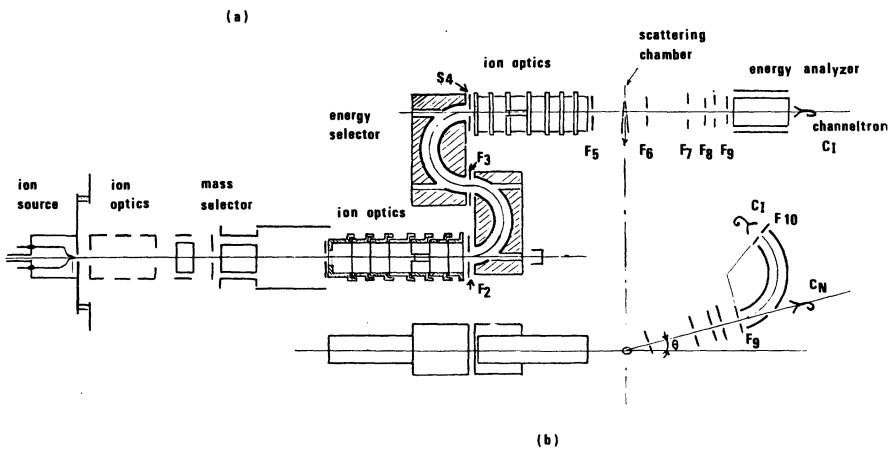

FIG. 1. Schematic description of the spectrometer used for ion scattering analysis, (a) side view, (b) top view.

= 2.5 mm. When the ions travel across the selector with energy $\epsilon = 20$ eV, a typical resolution of $\Delta E \simeq 80$ meV is obtained. A system of electrostatic lenses is then used to accelerate the He^+ ions up to the collision energy E_0 (laboratory frame) just before the collision chamber which is filled with the target gas at room temperature. In the present apparatus the collision energy can be varied from 50 eV up to 1 keV. The ions scattered at a given angle θ (laboratory frame) are selected by two slits F_6 and F_8 having a width of 0.6 and 0.4 mm, respectively. The angular spread of the scattered beam is $\Delta\theta \simeq 0.3°$.

The ions are then decelerated again before entering a 127° cylindrical electrostatic analyzer: The deceleration voltage is adjusted to get the required energy resolution which is just limited by the incident ion beam energy spread. The energy-loss spectrum is obtained by using an additional variable voltage superimposed on the deceleration voltage. The ions are detected by a channel multiplier. The counts are stored in a multichannel analyzer monitored by a microprocessor. Two types of energy-loss spectra (ELS) have been obtained and are as follows.

(i) "Low"-resolution ELS: The scattered ions are decelerated down to $E = 50$ eV (100 eV); the corresponding energy resolution attained for the analysis, $\Delta E = 0.2$ eV ($\Delta E = 0.4$ eV) is generally sufficient to resolve the *electronically* excited states of the molecule.

(ii) "High"-resolution ELS: The He^+ scattered ions can also be decelerated down to $E = 20$ eV, which improves the energy resolution at $E = 50$ eV (100 eV) by a factor of 2.5 (5), enabling the resolution of the *vibrational* levels of the M_2 molecule to be achieved.

The total intensity of neutral He produced by charge exchange is measured with an additional channel multiplier. Such measurements enable the determination of the relative probability of charge exchange $P_e(\theta) = N(\theta)/[N(\theta) + I(\theta)]$. This is achieved by measuring the total number of scattered particles $(N+I)$ with the analyzer voltage off and the number of neutrals (N) with the analyzer voltage on. These calibration experiments have to be run without decelerating the scattered ions after the collision in order to preserve the ions-to-neutrals ratio produced by the collision.

B. Charge-exchange processes: $He^+(1s^2S) + M_2(X) \rightarrow He(1s^{2\,1}S) + M_2^{+*}$ or $He^+(1s^2S) + M_2(X) \rightarrow He^*(1s,n1) + M_2^+$

The corresponding measurements are performed using the time of flight (TOF) technique. Since the experimental setup has been described previously,[19] only a few typical working conditions will be given. The flight length can be varied from 1.25 to 7.50 m depending upon the collision energy. The best energy resolution ($\Delta E \simeq 0.3$ eV) is limited by the ion source energy spread. Although this energy spread remains too large to resolve the individual vibrational levels of M_2^+, it enables the identification of a number of electronic states and the determination of the envelope of their vibrational distribution. The (He^+-He) system is used as a reference for the ELS measurements. The energy position of the He peak corresponding to the resonant-charge-exchange process determines the $Q = 0$ eV energy-loss origin of the spectra. The FWHM (full width at half maximum) of the He peak measures the energy resolution.

C. Cross sections

In analogy with ion-atom collisions, some $\sigma(\theta)$ differential cross sections (DCS) are conveniently presented in terms of the reduced cross section: $\rho(\tau) = \sigma(\theta)\theta \sin\theta$ as a function of the reduced angle $\tau = E_0\theta$. The $\rho(\tau)$ plot turned out to be useful in previous ion-molecule studies.[5(d)] For a particular process i the reduced DCS ρ_i and/or the relative excitation probability P_i are obtained by measuring the relative areas under the peaks in the ELS, and are calibrated by using the previously measured $P_e(\theta)$.

III. He^+-N_2 COLLISIONS

A. Energy-loss spectra—Direct excitation

Two types of excitation processes of the molecule have been investigated, namely: (i) the vibrational excitation of the ground state

$$He^+(1s^2S) + N_2(X\,^1\Sigma_g^+, v=0) \rightarrow He^+(1s^2S) + N_2(X\,^1\Sigma_g^+, v'),$$

and (ii) the electronic excitations of N_2:

$$He^+(1s^2S) + N_2(X\,^1\Sigma_g^+, v=0) \rightarrow He^+(1s^2S) + N_2^*(v').$$

1. Vibrational excitation of the ground state

Figure 2 shows a typical high-resolution ELS exhibiting eight vibrational levels of $N_2(X\,^1\Sigma_g^+)$. The relative intensity of the vibrational states has been investigated as a function of both the reduced angle τ and the collision energy E. At small scattering angles the angular spread of the incident beam prevents an unambiguous determination of the $v = 0$ elastic peak intensity. The results of these measurements, summarized in Table I, show the *decrease of vibrational excitation* with increasing energy. Furthermore, the present data show that $N_2(X\,^1\Sigma_g^+)$ vibrational excitation remains quite small ($\leq 10\%$ for $E_0 \geq 200$ eV) in the explored τ range.

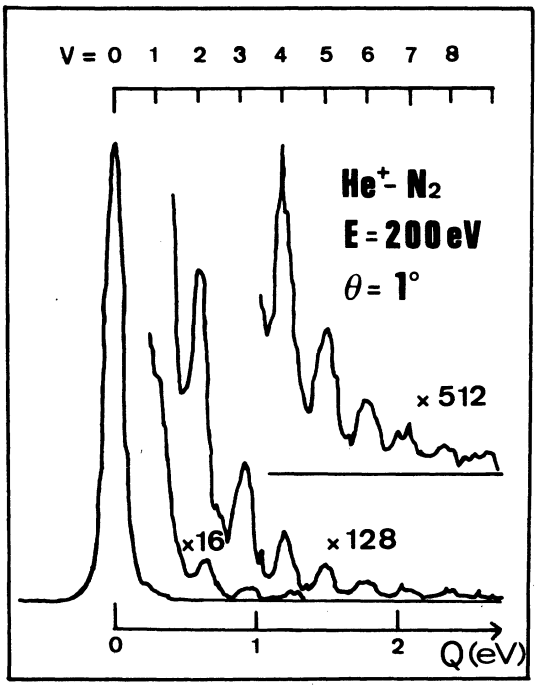

FIG. 2. ELS of scattered He^+ from He^+-N_2 collision showing weak excitation of the resolved vibrational levels of the N_2 ground state.

This finding is most significant as it implies the validity of the Franck-Condon principle when studying electronic excitation in this system for $E \geq 200$ eV.

2. *Electronic excitation of N_2*

Figure 3 shows some typical ELS exhibiting electronic excitation of N_2. The proposed identification of the structure in the spectra is obtained using the energy curves of Fig. 4(a) in the Franck-Condon region,

X:	$Q = 0$ eV elastic scattering.	
α:	$7.8 \leq Q \leq 8$ eV,	$B\,^3\Pi_g (v = 2, 3)$
β:	$8.5 \leq Q \leq 10.5$ eV,	A group of electronic states may contribute to this structure—$a\,^1\Pi_g$, $B'\,^3\Sigma_u^-$, $a'\,^1\Sigma_u^-$, $w\,^1\Delta_u$.
γ:	$Q \simeq 11.1$ eV,	$C\,^3\Pi_u (v = 0, 1)$
δ:	$Q \simeq 12$ eV,	$E\,^3\Sigma_g^+$
ϵ:	$Q \simeq 13.2$ eV,	$b\,^1\Pi_u$ (see Refs. 22–24)
ϕ:	$Q \simeq 14$eV,	$b'\,^1\Sigma_u^+$ (see Refs. 22–24)
χ:	$15.6 \leq Q \leq 27$ eV.	

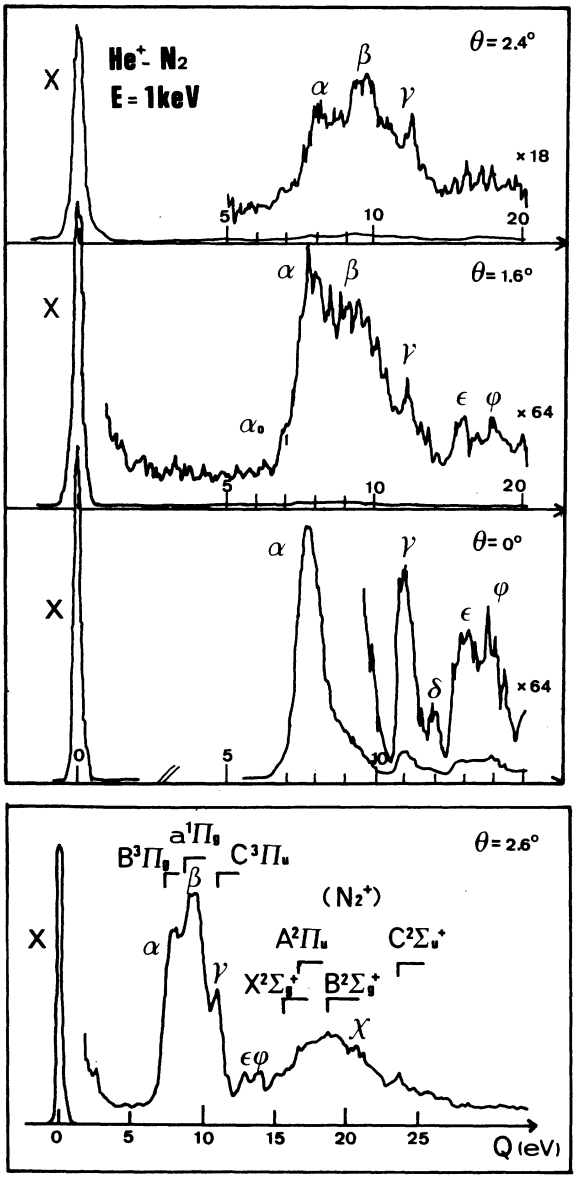

FIG. 3. Low-resolution ELS of scattered He^+ from He^+-N_2 collision. The peaks labeled $X, \alpha, \beta, \gamma, \delta, \epsilon, \phi, \chi$ refer to elastic scattering (X) and excitation of electronic states of N_2. (See text and Table II for molecular state identification.)

In the Franck-Condon region, the $N_2(A\,^3\Sigma_u^+)$ and $N_2(B\,^3\Pi_g)$ states may contribute to peak α. The excitation of the $A\,^3\Sigma_u^+$ state should lead to a maximum at $Q \simeq 7.5$ eV. To remove this ambiguity, a high-resolution spectrum has been studied at small angle. In this spectrum, Fig. 5, the resolved vibrational structure of peak α is unambiguously identified as the vibrational distribution of the $B\,^3\Pi_g$ ($v = 0, 1, \ldots, 7$) state. The shoulder α_0 on the side of peak α at large angles (Fig. 3) might

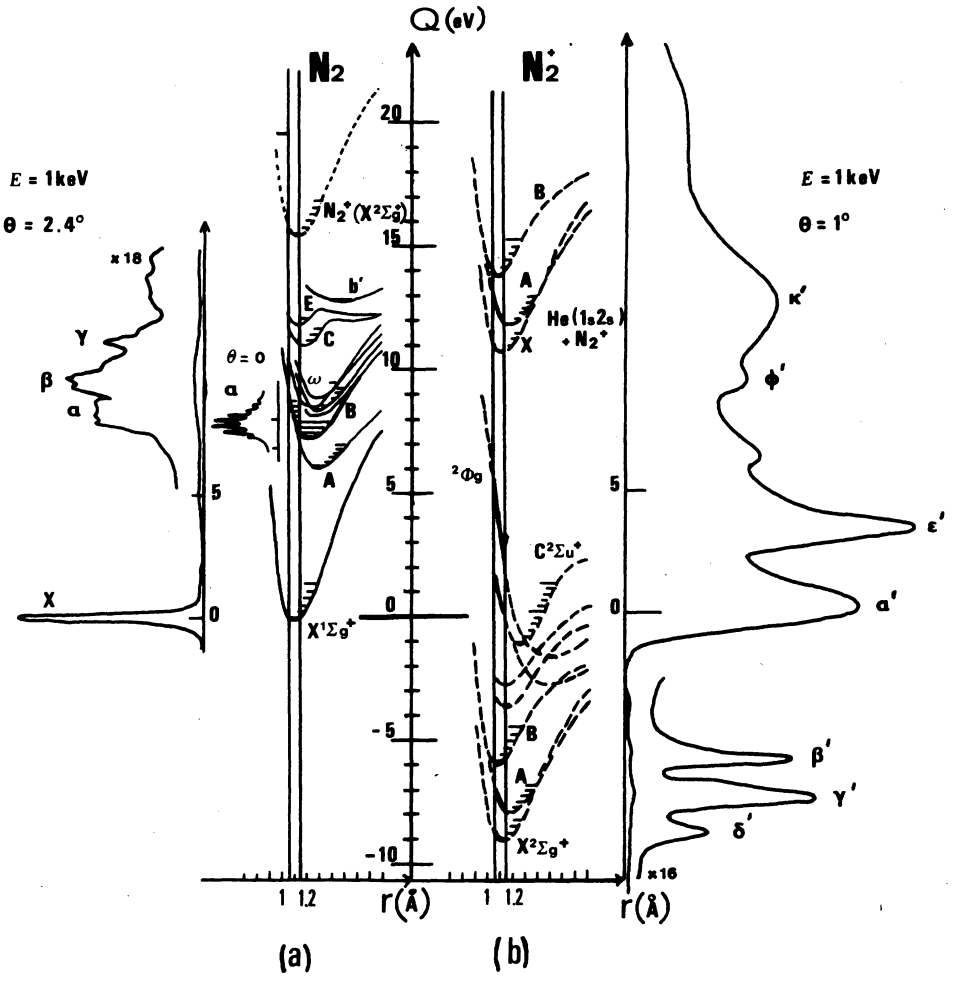

FIG. 4. Potential-energy curves for (a) N_2 (Ref. 20) and (b) N_2^+ (Refs. 20 and 21) are displayed in the Franck-Condon region, together with typical ELS for direct and exchange processes. The origin of the energy scale corresponds to the incident channel $[He^+(1s)+N_2(X)]$.

be attributed to a weak excitation of $N_2 A\,^3\Sigma_u^+$. It should be stressed that the good agreement between the measured relative intensities of the vibrational levels of the $B\,^3\Pi_g$ state with those predicted from Franck-Condon overlap factors (Fig. 5) is another argument (see Sec. V) in favor of the applicability of "FC vertical transitions".

Figure 3 shows that the main structures of the

TABLE I. Relative probabilities $P_0=P_v/\sum_{v=0}^{v=5} P_v$ of vibrational excitation of the N_2 ground state for various collision energies. For 500-eV energy the $v=0$ level could not be completely separated from the incident beam therefore, only the relative intensity $P_v/(P_{v=1})$ is given.

E	100 eV		200 eV		500 eV	
θ (deg)	1	2	1	2	0.2	0.6
v	P_0	P_0	P_0	P_0	P_1	P_1
0	0.91	0.84	0.96	0.88		
1	6×10^{-2}	0.11	2.4×10^{-2}	9×10^{-2}	1	1
2	1.4×10^{-2}	2.7×10^{-2}	5.4×10^{-3}	1.6×10^{-2}	0.14	0.17
3	7×10^{-3}	1.8×10^{-2}	3×10^{-3}	7×10^{-3}	0.05	0.07
4	3×10^{-3}		1.3×10^{-3}	4.7×10^{-3}	0.02	0.03
5			5×10^{-4}	3×10^{-3}	0.01	0.02

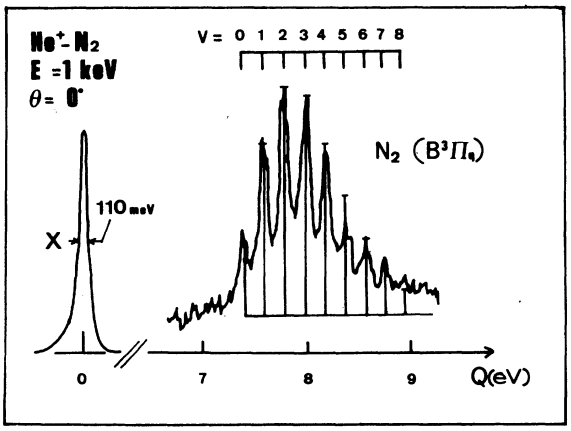

FIG. 5. High-resolution ELS of scattered He^+ at small angle. The vibrational excitation of the $N_2(B\,^3\Pi_g)$ state is compared with the predicted Franck-Condon distribution (vertical bars): The two distributions are normalized for the $v=2$ level.

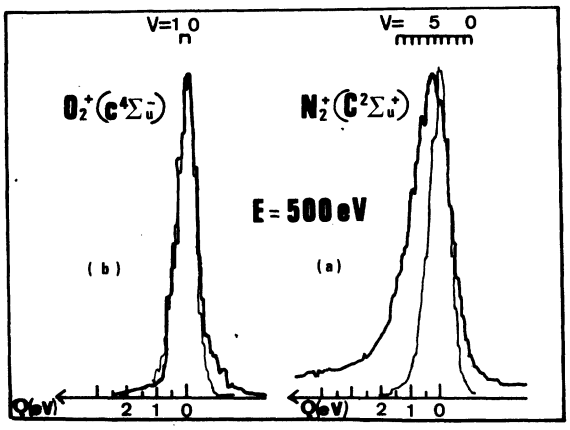

FIG. 6. ELS of scattered neutral He from He^+-N_2 collision (a) and He^+-O_2 collision (b) at small reduced angle τ. The single peak observed corresponds to near-resonant electron-capture process. The profile of the quasiresonant charge-exchange-process peak (α) for both systems is compared to the profile of the resonant charge-exchange-process peak for He^+-He system under the same (E,θ) conditions (light line). Peak α' relative to the He^+-N_2 collision (thick line) is much broader than the reference peak showing the excitation of several vibrational levels of $N_2^+(C\,^2\Sigma_u^+)$ state. In contrast, peak α' relative to the He^+-O_2 collision is nearly identical to the reference peak exhibiting the excitation of only one or two vibrational levels of $O_2^+(C\,^4\Sigma_u^-)$ state.

spectra correspond to processes X, α, β, γ, and χ. Peak $\alpha(B\,^3\Pi_g$ state) is the dominant direct excitation process at the lowest τ values. With increasing τ, peak β shows up rapidly. The broad structure χ occurring at higher-energy losses can be ascribed to both ionization[5(c)] of the N_2 molecule [ionization potential (IP) = 15.6 eV] and excitation of Rydberg states $N_2^*(R)$.[25] Such Rydberg series converge towards the ground state $(X\,^2\Sigma_g^+)$ and excited states $(A\,^2\Pi_u,\ B\,^2\Sigma_u^+\cdots)$ of N_2^+. Inspection of the ELS for energy losses $Q \geq 40$ eV shows no structure indicating that no He^+ excitation occurs.

B. Energy-loss spectra: Electron-capture processes

At low energy $E=200$ eV and small angles $(0<\theta<1°)$ a single peak α' is observed [Fig. 6(a)] at an energy loss $Q\simeq 0.3$ eV. This structure certainly corresponds to the quasiresonant charge-exchange process:

$$He^+(1s\,^2S)+N_2(X\,^1\Sigma_g^+) \rightarrow He(1s\,^2S)+N_2^+(C\,^2\Sigma_u^+,\ v_{max}=5,6)\,.$$

The measured $\delta E=1.3$ eV (FWHM) of the peak is broad compared to the reference peak (i.e., resonant-charge-transfer peak of the $He^+ + He$ system: $\delta E\simeq 0.6$ eV) which demonstrates that several vibrational states are excited. Actually, the $C\,^2\Sigma_u^+$ state has been observed in ESCA (electron spectroscopy for chemical analysis) and photoelectron spectroscopy.[26] In these experiments excitation of the $v=4$ to 10 levels with a maximum intensity around $v=6$ as predicted by the FC principle is observed and is consistent with the present results.

A single dominant charge-exchange peak was found by Hodge *et al.*[10] (for $0.5\ \text{keV}\leq E\leq 1\ \text{keV}$, $0.25°\leq\theta\leq 2°$) and interpreted by these authors as due to the above near-resonant-charge-exchange process. Figure 8 actually shows that in the τ range investigated by Hodge *et al.* other charge-exchange channels are strongly populated.

The salient feature of TOF spectra (Fig. 7) is the strongly unbalanced excitation of exothermic and endothermic channels.

i. Exothermic channels ($Q\leq 0$). Although the relative intensity of the observed peaks remains very small, they are easily resolved. The following identification of the peaks in Fig. 7 is proposed:

$$\left.\begin{array}{ll}\beta': & -5.5\ \text{eV}\leq Q\leq -6\ \text{eV},\quad N_2^+(B\,^2\Sigma_u^+, v=0,1)\\ \gamma': & Q=-7.5\ \text{eV},\quad N_2^+(A\,^2\Pi_u, v=2,3)\\ \delta': & Q=-9\ \text{eV},\quad N_2^+(X\,^2\Sigma_g^+, v=0,1)\end{array}\right\} + He(1s^2\,^1\Sigma)\,.$$

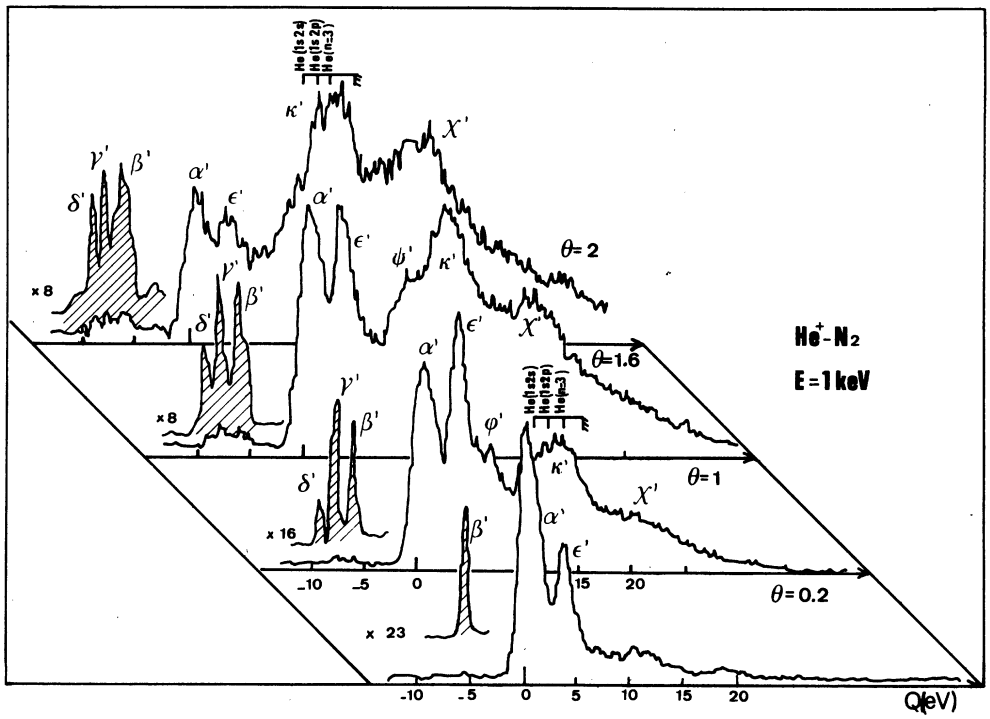

FIG. 7. ELS of scattered He from He^+-N_2 collision: The striking features are (i) when τ increases, *a number of* exothermic and endothermic channels are excited, and (ii) the ELS display a strong asymmetry—the exothermic channels are weakly excited, whereas excitation of endothermic channels (κ' and χ') become dominant when τ increases. The identification of the peaks (β', γ', δ') and ($\epsilon', \psi', \kappa', \chi'$), respectively, are given in the text.

Consistent with the Wigner spin-conservation rule, no structure is observed which corresponds to population of $N_2^+(^4\Sigma_u^+)$.

ii. Endothermic channels $Q>0$. The excitation of these channels starts at $\tau \geq 0.3$ keV deg and contrary to the behavior of exothermic channels they increase strongly with increasing τ and E. Peak ϵ' ($Q \simeq 3.5$ eV) could not be identified using the compilation of Gilmore.[20] Referring to the *ab initio* calculations of Cartwright and Dunning[21] there are four states of N_2^+: $^2\phi_g$, $^2\Pi_g$, $^2\Delta_u$, and $^2\Sigma_u^-$ in the FC region that might be candidates for the observed energy loss. Among these states, the $^2\phi_g$ state is singled out by the FC principle and would best account for the ϵ' peak. An alternative identification of this peak is provided by the calculations of Herman *et al.*[27] that suggest the existence of a $^2\Pi_u$ state 3.3 eV above the $C\,^2\Sigma_u^+$ state. This candidate would nicely account for the ϵ' peak.

The shoulder ϕ' on the side of the ϵ' peak (around $Q \sim 6$ eV) could not be clearly identified since the corresponding energy range in the N_2^+ level diagram is crowded by several states. Furthermore the energy-level diagram of N_2^+ is not known well enough to provide the identification of the structure ψ' at $Q \simeq 8.5$ eV. However, calculations by Herman and Freed[27] show the existence of a $^2\Pi_g$ state about 8 eV above the $C\,^2\Sigma_u^+$ state that might account for peak ψ'.

The broad peak κ' at 10.5 eV $\leq Q \leq$ 15.6 eV corresponds to the electron capture into excited states of He, according to

$$He^+(1s\,^2S) + N_2(X\,^1\Sigma_g^+) \rightarrow He(1s2l) + N_2^+(X\,^2\Sigma_g^+),$$
$$10.8 \text{ eV} \leq \Delta E \leq 13.7 \text{ eV},$$
$$He^+(1s\,^2S) + N_2(X) \rightarrow He(1snl) + N_2^+(X),$$
$$13.7 \text{ eV} \leq \Delta E \leq 15.6 \text{ eV}.$$

The maximum intensity of this structure lies around 11.5 eV at $E=1$ keV (He, $n=2$) and around 14 eV at $E_0=2$ keV (He, $n=3$ up to ionization). This identification is supported by the experiments of Gochitashvily *et al.*[28] who observed, in the 0.2-keV $\leq E \leq$ 1-keV energy range, He I lines corresponding to significant electron capture into $He(3\,^{3,1}D,\ 3\,^3S,\ 4\,^{3,1}D,\ 4\,^1S)$. In the absence of knowledge of N_2^{+*} Rydberg states it is difficult to decide whether the structure κ' might contain processes of the type

$$He^+(1s\,^2S) + N_2(X) \rightarrow He(1s^2\,^1S) + N_2^{+*}(R).$$

However, this possibility should be kept in mind.

The broad peak χ' (18 eV $\leq Q \leq$ 24 eV) with a width

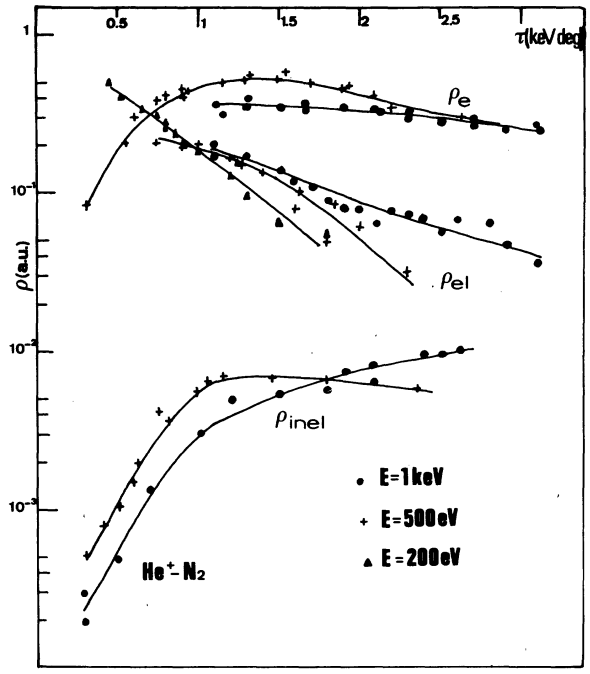

FIG. 8. Reduced differential cross sections for the He^+-N_2 collision as a function of the reduced scattering angle. The curves labeled ρ_e, ρ_{el}, and ρ_{inel} refer to charge-exchange processes, elastic scattering, and inelastic scattering corresponding to electronic excitation of N_2, respectively. The different energy sets of DCS have been adjusted for $\tau = 1$ keV deg. Charge-exchange processes are seen to be dominant.

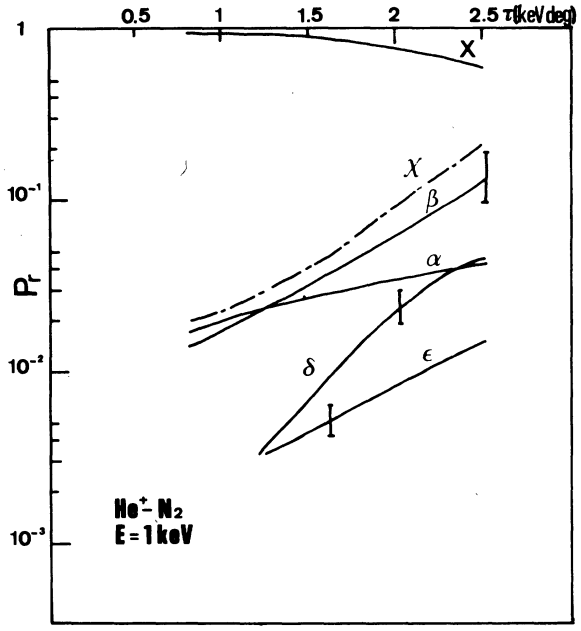

FIG. 9. Relative probabilities P_r of direct electronic excitation of N_2 by He^+ impact, as a function of the reduced scattering angle. X refers to elastic scattering and the $\alpha, \beta, \gamma, \epsilon, \chi$ curves refer to the various electronic excited N_2^* states the identification of which is given in the text.

similar to that of the κ' peak should correspond to two-electron excitation:

$$He^+(1s\,^2S) + N_2(X) \rightarrow He^*(1snl) + N_2^{+*}.$$

This peak is clearly superimposed on a tail corresponding to the transfer ionization channel

$$He^+(1s\,^2S) + N_2(X) \rightarrow He(1s^2\,^1S) + N_2^{2+} + e, \quad \Delta E \geq 18.1 \text{ eV}.$$

At higher energy (4 keV) a third broad peak appears around $Q \simeq 30$ eV that might correspond to autoionizing dissociative N_2^{+**} states.

C. Relative probabilities of collision processes

The relative importance of total charge exchange and total direct excitation of the N_2 molecule has been measured (Fig. 8) for $E = 200$ and 500 eV, and (1 keV). *The salient feature of the data is the dominance of charge-exchange processes.*[5(f)] Figures 9 and 10 show the relative probabilities for the population of the various channels discussed above.

The quasiresonant charge-exchange process is found to be dominant for the small τ values; the relative population of the *exothermic* channels (β', γ', δ') remains quite small over the range of τ investigated, whereas the endothermic channels (κ', χ') become dominant with increasing τ. Since the ρ_e cross section remains nearly constant the behavior of the relative excitation probabilities means that the quasiresonant channel suffers a strong absorption by the other charge-exchange channels when τ increases. Figure 11 exhibits the dependence of *relative excitation probabilities* as a function of the collision energy E_0 for various charge-exchange channels. This figure shows a strong increase with energy (*dynamic* effect) of the exothermic process β' and, to a lesser extent, of the endothermic process χ'. In contrast, the relative probability of excitation for the quasiresonant process α' and for process ϵ' slowly decrease with energy.

IV. He^+-O_2 COLLISION

A. Energy-loss spectra: Direct excitation

Vibrational excitation of the O_2 ground state has also been investigated and found very small as in the He^+-N_2 collision. Direct electronic excitation of O_2 has been measured at $E_0 = 0.5$ and 1 keV:

$$He^+(1s^2S) + O_2(X\,^3\Sigma_g^-) \rightarrow He^+(1s^2S) + O_2^*(v').$$

Figure 12 shows some typical ELS, the five structures of which are identified using the compilation of Gilmore[20] and *ab initio* potential-energy curves

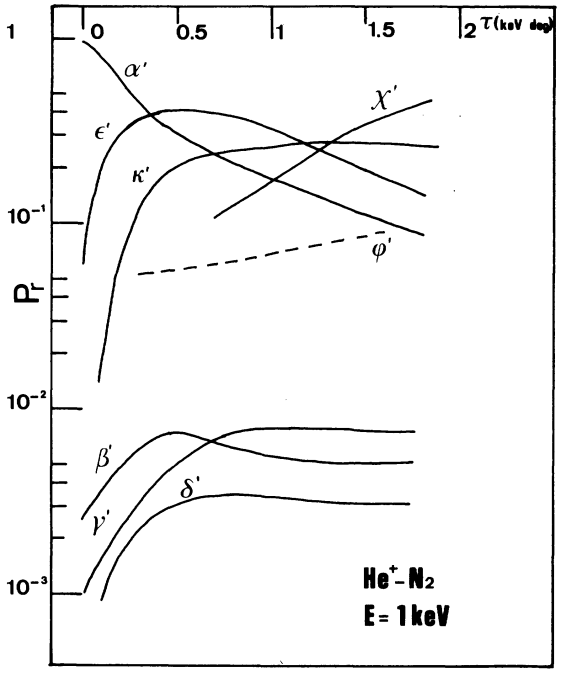

FIG. 10. Relative probabilities P_τ of charge-exchange-channel population as a function of the reduced scattering angle. The curves labeled α', $(\epsilon', \kappa', \chi')$, and $(\beta', \gamma', \delta')$ refer to quasiresonant charge-exchange process, excitation of endothermic channels, and excitation of exothermic channels, respectively. The quasiresonant electron-capture process is dominant at low τ, but the endothermic channels population (κ', χ') increases strongly with increasing τ. The exothermic channels remain weakly excited.

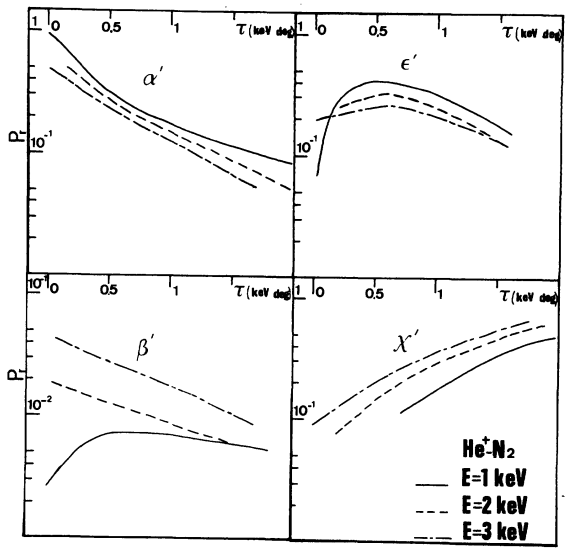

FIG. 11. Dependence with energy of the relative excitation probabilities P_τ of some typical charge-exchange channels. The salient features are (i) the strong dynamic effect for the excitation of exothermic process β', (ii) the relative decrease of the population of α' and ϵ' channels, and (iii) the increasing dominance of the endothermic processes κ' and χ' for the large-τ values.

of Saxon *et al.*[29] [Fig. 13(a)]:

X: $Q=0$ elastic scattering
α: $Q=1$ eV O_2 ($a\,^1\Delta_g$ $v=0$)
β: $Q=1.6$ eV O_2 ($b\,^1\Sigma_g^+$ $v=0$)
γ: $5.3\ \text{eV} \leq Q \leq 7$ eV (the three $A\,^3\Sigma_u^+$, $C\,^3\Delta_u$, $C\,^1\Sigma_u^-$ states associated with the same electronic configuration may contribute to this peak whose maximum is located at 6 eV.)
δ: $7\ \text{eV} \leq Q \leq 9.5$ eV (with $Q=8$ eV at the location of the peak).

Several electronic states may account for the structure δ, as seen from Fig. 13. The $B\,^3\Sigma_u^-$ (Schuman-Runge continuum) the $^{3,1}\Pi_g(V)$ valence states and the $^3\Pi_g(R)$ lowest Rydberg state of O_2, which has been investigated by e impact experiments.[30] The weak excitation of the higher $^3\Sigma_u^-(R)$ Rydberg state may be responsible for the shoulder observed around the 9.5-eV energy loss.

It is noteworthy that peaks α and β have nearly the same FWHM ($\delta E \simeq 0.4$ eV) as the elastic peak whereas peaks γ and δ have a width of 1.8 and 2.5 eV, respectively. This striking difference is related to the shape of the relevent potential-energy curves in the FC region. Indeed, the $a\,^1\Delta_g$ and $b\,^1\Sigma_g^+$ states as well as the $X\,^3\Sigma_g^-$ ground state have the same electronic configuration and present a well at the same equilibrium distance ($re \simeq 1.15$ Å): The dominant excitation of the $v=0$ level of the a and b states is, therefore, consistent with the FC prediction. On the other hand, the $A\,^3\Sigma_u^+$ and $B\,^3\Sigma_u^+$ states, which are strongly repulsive in the FC region, lead to a broad structure. It is noteworthy that, contrary to the He^+-N_2 case, no significant ionization of O_2 is observed.

B. Energy-loss spectra: Electron-capture processes

Similar ELS (for $100\ \text{eV} \leq E \leq 300$ eV) have been recently published by Gillen.[11] For small-τ values the spectrum is dominated by a single peak α' associated with a $Q \simeq 0$-eV energy loss (Fig. 6). Quasiresonant electron capture into the $c\,^4\Sigma^-$ (Ref. 31) and $^2\Pi_u O_2^+$ states might contribute to peak α'. However, the $\delta E = 0.6$ eV FWHM of peak α' which is identical to that of the He^+-He reference peak (Fig. 6) strongly suggests that the quasiresonant charge-exchange process is mainly due to the population of the O_2^+ $c\,^4\Sigma_u^-$ state. Indeed, it is seen on

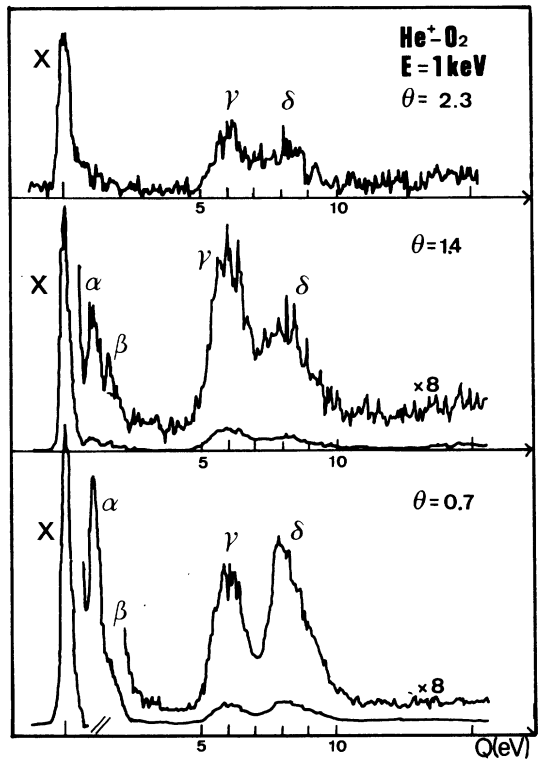

FIG. 12. Low-resolution ELS of scattered He^+ from He^+-O_2 collisions. The peaks labeled $X, \alpha, \beta, \gamma, \delta$ refer to elastic scattering (X) and excitation of electronic states of O_2 (see text and Table II for molecular state identification).

Fig. 13 that only the two $v=0$ and $v=1$ vibrational levels of the quasibound $c\ ^4\Sigma_u^-$ state lie in the FC region and should be excited. On the other hand the $^2\Pi_u$ state should give rise to a broader structure (2 eV). Yet excitation of this state can account for the very weak tail for $Q<0$ (Fig. 6).

For larger τ and energy values, the ELS displayed in Fig. 14 show that the He^+-O_2 charge-exchange spectra present the same salient features as those of the He^+-N_2 system: a strong excitation of endothermic channels compared to a weak excitation of exothermic channels.

i. Exothermic channels. $He^+(1s\,^2S)+O_2(X\,^3\Sigma_g^-) \rightarrow He(1s^2\,^1S)+O_2^{+*}$: Four structures can be resolved and are assigned as

β': $Q\simeq -4$ eV, $O_2^+(B\,^2\Sigma_g^-,\ v\simeq 2)$

γ': $Q\simeq -6.3$ eV, $O_2^+(b\,^4\Sigma_g^-,\ v\simeq 1)$

δ': $Q\simeq -7.5$ eV, $O_2^+(A\,^2\Pi_u$ and $a\,^4\Pi_u)$

ϕ': $Q\simeq -12$ eV, $O_2^+(X\,^2\Pi_g,\ v\simeq 3)$.

It is noteworthy that the observed structures account for *all* the electronic states of O_2^+ lying in the corresponding energy-loss range.

ii. Endothermic channels. The excitation of these channels exhibits the same τ dependence as the excitation of endothermic channels in He^+-N_2. Identification of peak ϵ' cannot be found in the compilation of Gilmore.[20] However, using O_2^+ *ab initio* energy curves[32] it is seen that the $^2\Sigma_u^-$ and $^2\Delta_u$ dissociative states of O_2^+ lie about 3 eV above the $c\ ^4\Sigma_u^-$ state in the FC region and might be responsible for location and broadness of structure ϵ'.

As in the He^+-N_2 collisions two additional broad peaks (κ', χ') would correspond to excitation of He Rydberg states with or without simultaneous O_2^{+*} excitation,

$$He^+(1s^2S)+O_2(X\,^3\Sigma_g^-) \rightarrow He^*(1s,nl)+O_2^+(X),$$

$$7\ \text{eV} \leq \Delta E \leq 12\ \text{eV},$$

$$He^+(1s^2S)+O_2(X\,^3\Sigma_g^-) \rightarrow He^*(1s,nl)+O_2^{+*}.$$

However, unlike the He^+-N_2 case where the structure κ' reflects the excitation of the whole $He(1snl)$ Rydberg series, the narrower structure κ' observed in He^+-O_2 favors the excitation of the lowest [$He(1s,\ 2s\,^{3,1}S)$] Rydberg states. As pointed out in Sec. III B this structure may as well reflect the excitation of channels of the type [$He(1s^2\,^1S)+O_2^{+*}(R)$] involving the yet unidentified $O_2^{+*}(R)$ Rydberg states. At higher energies, $E=2$-3 keV, a third broad peak is observed around $Q\approx 22$ eV. These large energy-loss structures are superimposed upon a broad tail corresponding to ionization charge transfer

$$He^+(1s^2S)+O_2(X\,^3\Sigma_g^-) \rightarrow He(1s^2\,^1S)+O_2^{2+}+e.$$

C. Relative probabilities of collision processes

Proceeding in the same way as in the He^+-N_2 case we have measured the relative probability of direct and electron-capture processes (Fig. 15). Here again the charge-exchange process is found to be dominant in the explored energy range. Figures 16 and 17, respectively, show the relative probabilities of direct electronic excitation channels of O_2, and those for the various charge-exchange channels.

V. DISCUSSION

A. General

The important features found in the ELS data demonstrate that for both the He^+-N_2 and He^+-O_2 systems:

(i) The energy losses of the well-identified channels correspond to the energy gaps between the potential-energy curves *in the FC region*.

(ii) The energy width of the observed peaks is clearly connected with the shape of the potential-

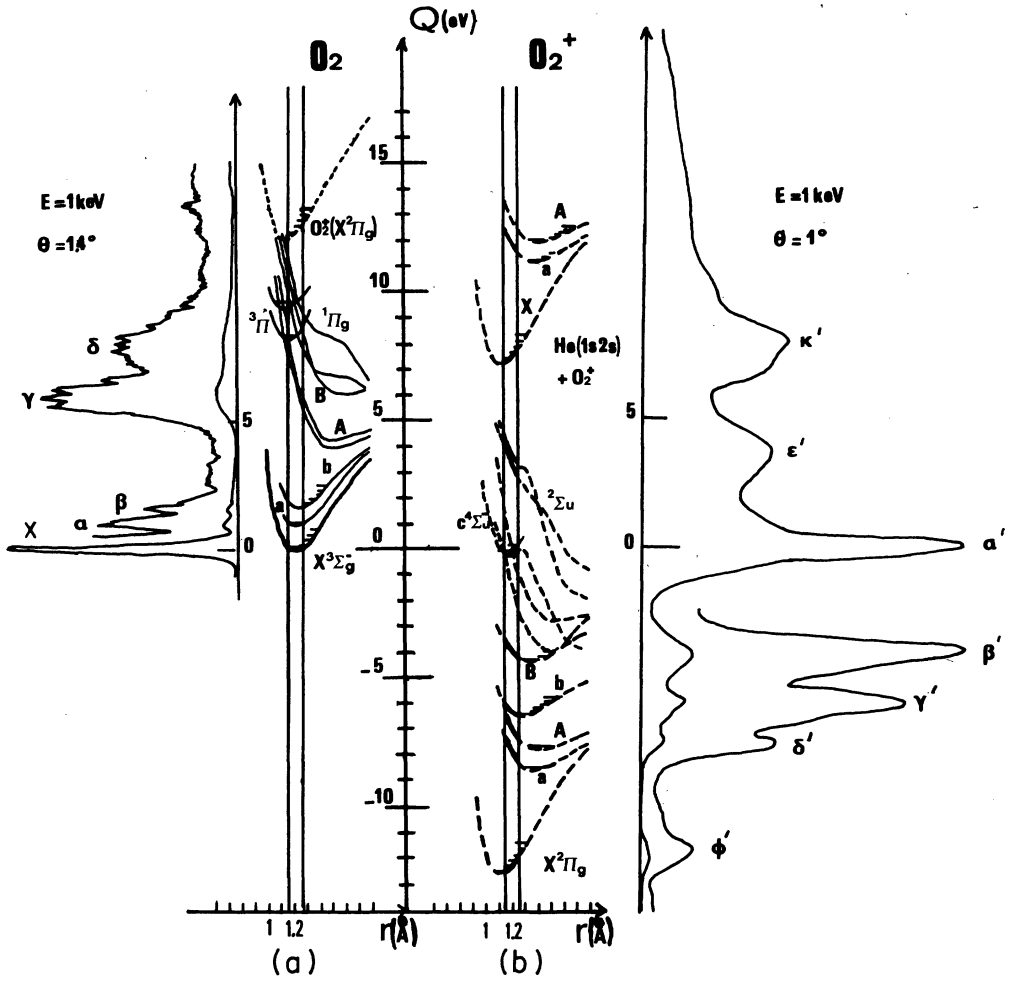

FIG. 13. Potential-energy curves for (a) O_2 (Ref. 20) and (b) O_2^+ are displayed in the Franck-Condon region, together with typical ELS for direct and exchange processes. The origin of the energy scale corresponds to the incident channel $[He^+(1s)+O_2(X)]$.

energy curves in the FC region; in particular, those energy levels having the same shape as the $M_2(X)$ ground state in the FC region give rise to narrow peaks [e.g., $O_2(a\,^1\Delta_g)$, $O_2(b\,^1\Sigma_g^+)$, O_2^+ $(c\,^4\Sigma_u^-)$], whereas all other cases lead to broad structures. Broad structures are encountered when many vibrational levels of a given electronic state lie in the FC region or when a dissociative molecular state is excited. For the well-isolated $N_2(B\,^3\Pi_g)$ state resolution of the vibrational structure demonstrates that the relative vibrational population obeys a FC distribution. These features, together with the absence of significant vibrational excitation of the X ground state of the molecule provide strong evidence for the cogency of the use of the FC principle for the considered systems under the explored experimental (E,θ) conditions for both direct-excitation and charge-exchange processes.

Synthesizing the data of Sec. III and IV, striking similarities of the collision processes in He^+-N_2 and He^+-O_2 systems emerge:

(i) a strong dominance of the quasiresonant charge-exchange process at small τ.

(ii) a striking asymmetry in the population of the nonresonant charge-exchange channels; for a similar energy defect endothermic processes are much more enhanced than exothermic processes.

(iii) the relative population of exothermic channels show a significant dependence on energy which suggests a strong dynamic effect.

(iv) electron-capture processes dominate direct-excitation processes.

These features strongly resemble those encountered in He^+–rare-gas (RG) collisions suggesting

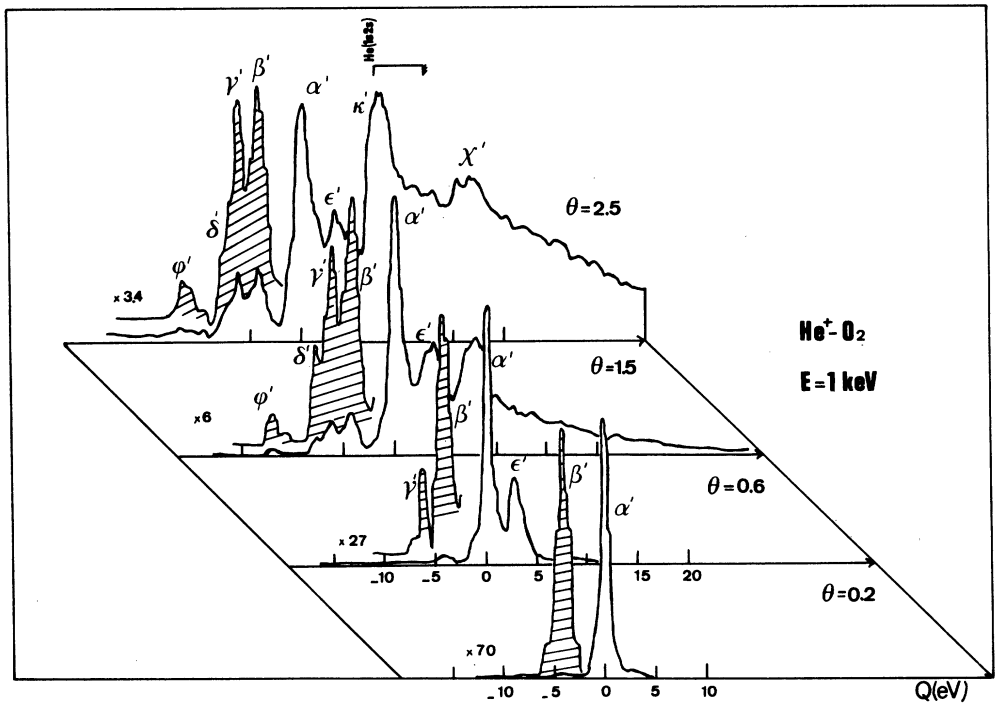

FIG. 14. ELS of scattered He from He^+-O_2 collision. The same asymmetry between the exothermic channels weakly populated and the endothermic channels becoming dominant at large τ as in the He^+-N_2 case is observed.

similar qualitative excitation mechanisms. Actually these similarities will be seen to reflect a common character of the electronic structure of all these systems, namely, the initial vacancy in the 1s He orbital becomes an inner vacancy in the quasimolecule $(He\text{-}M_2)^+$ and $(He\text{-}RG)^+$ formed during the collision. All the target orbitals up to $3\sigma_g$ and $1\pi_u$ are completely filled. This confers a rare-gas-like electronic structure to N_2; however, O_2 has two additional outer electrons ($1\pi_{gx}$ and $1\pi_{gy}$)

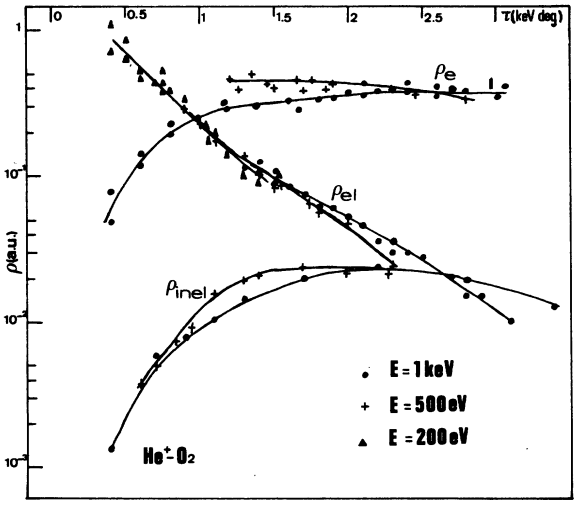

FIG. 15. Reduced differential cross sections for the He^+-O_2 collision as a function of the reduced scattering angle. The curves labeled ρ_e, ρ_{el}, and ρ_{inel} refer to charge-exchange processes, elastic scattering, and inelastic scattering corresponding to electronic excitation of O_2, respectively. The different energy sets of DCS are adjusted for $\tau = 1$ kev deg.

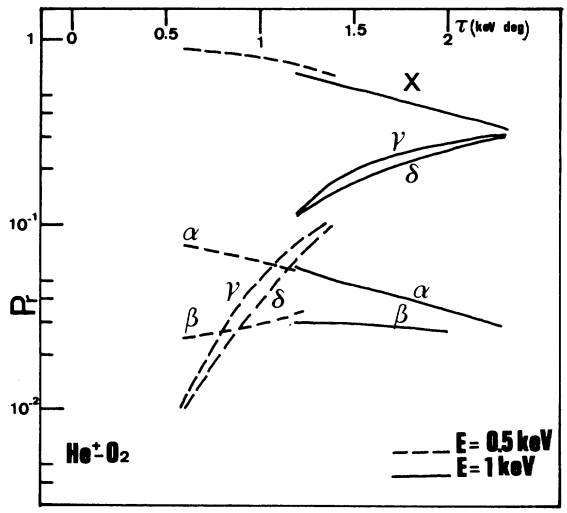

FIG. 16. Relative probabilities P_τ of direct electronic excitation of O_2 in He^+-O_2 collision, as a function of the reduced scattering angle τ. X refers to elastic scattering and the $\alpha, \beta, \gamma, \delta$ curves refer to the various electronically excited O_2^* states the identification of which is given in the text.

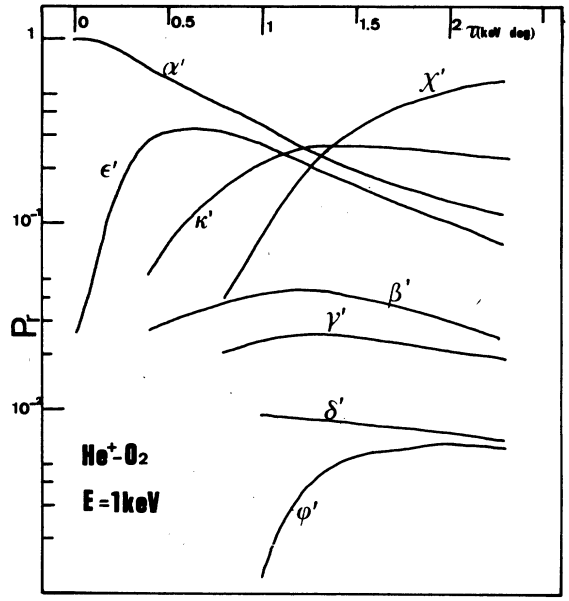

FIG. 17. Relative probabilities P_r of charge-exchange-channel population as a function of the reduced scattering angle. The curves labeled α', $(\epsilon', \kappa', \chi')$ and $(\beta', \gamma', \delta', \phi')$ refer to quasiresonant charge-exchange-process excitation of endothermic channels and excitation of exothermic channels, respectively. The quasiresonant electron-capture process is dominant at low τ; the population of endothermic channels (χ', κ') increases with increasing τ, whereas the exothermic channels remain weakly excited.

whose degeneracy is lifted in the quasitriatomic molecule. The consequence of this difference is that in the He^+-N_2 collisions the entrance channel $[He^+(^2S) + N_2(X\,^1\Sigma_g^+)]$ has the $^2A'$ symmetry, whereas in the He^+-O_2 collision $[He^+(^2S) + O_2(^3\Sigma_g^-)]$ both $^2A''$ and $^4A''$ symmetry entrance channels are formed in the statistical ratio. (The symmetry species refers to the most general Cs symmetry point group of a triatomic molecule). Table II lists the observed processes and their possible assignments along with the corresponding electronic configurations as taken from literature.

B. Quasiresonant and exothermic processes: Direct-transition mechanisms

The quasiresonant process α' ($Q \leq 0.5$ eV) in both the He^+-N_2 and He^+-O_2 systems appearing at the smallest values of τ is certainly responsible for the large total charge-exchange cross sections (10^{-15} cm^2) previously measured.[17] Since these studies show that total charge exchange in the systems considered yields essentially $(N^+ + N)$ and $(O^+ + O)$ products, our assignment of peak α' confirms that the $N_2^+(C\,^2\Sigma_u^+)$ and $O_2^+(c\,^4\Sigma_u^-)$ state, respectively, are dissociative or strongly predissociated. In He^+-O_2, the $c\,^4\Sigma_u^-$ state is formed by a $(a'_{2\sigma_u} \rightarrow a'_{1s\,He})$ one-electron transition. On the other hand, in He^+-N_2 two-electron configurations[20,27] contribute to the $N_2^+(C\,^2\Sigma_u^-)$ state; that corresponding to the $(a'_{2\sigma_u} \rightarrow a'_{1s\,He})$ one-electron transition has the smaller weight. The other configuration $[(2\sigma_u)^2(1\pi_u)^3(3\sigma_g)^1(1\pi_g)^1]$ is obtained as a result of a correlated two-electron jump: one electron filling the 1s He vacancy and the other being excited into the $(1\pi_g)$ orbital. This process is favored by the quasiresonance and should occur at large intermolecular distances.

Table II also shows the excitation of electronic states generated by one-electron transitions from the successive valence orbitals of the molecule to the 1s He orbital. The strong dynamic effect of such reactions suggests a mechanism similar to the so-called Demkov model[33] used for ion-atom collisions. This model predicts a charge-exchange-transition probability of the form

$$P \approx 2\exp\left(-\frac{\pi\sqrt{2}}{v}\,\frac{\Delta\epsilon}{(\sqrt{I_1}+\sqrt{I_2})}\right), \qquad (2)$$

where I_1 and I_2 are the binding energies of the electron in the initial and final states, $\Delta\epsilon$ is the corresponding energy splitting and v is the colli-

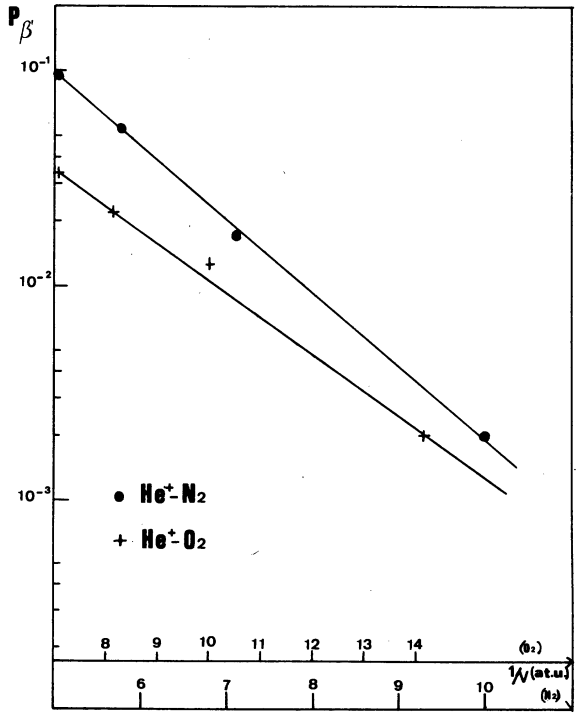

FIG. 18. $P\beta'$ represents the probability of direct transition of one electron from the incident channel to the $[He(1s^2) + M_2^+(\beta')]$ exchange channel. $\log P\beta'$ for He^+-N_2 (•) and He^+-O_2 (+) collisions shows a quasilinear dependence as a function of $1/v$, where v is the collision velocity, in the explored energy range.

TABLE II. Identification of inelastic processes in the He^+-N_2 and -O_2 systems.

(a) $He^+ - N_2$

Observed process Direct	N_2 excitation	Electronic configuration $(2\sigma_u)$	$(3\sigma_g)$	$(1\pi_u)$	$(1\pi_g)$	$(n\Lambda)$	$(He-N_2)^+$ Quasimolecular symmetry
X	$X\,^1\Sigma_g^+$	2	2	4	0		$^2A'$
α	$B\,^3\Pi_g$	2	1	4	1		$^{2,4}A'$, $^{2,4}A''$
β	$a\,^1\Pi_g$	2	1	4	1		$^2A'$, $^2A''$
	$B'\,^3\Sigma_u^-$	2	2	3	1		$^2A''$, $^4A''$
	$a'\,^1\Sigma_u^-$	2	2	3	1		$^2A''$
	$\omega\,^2\Delta_u$	2	2	3	1		$^2A'$, $^2A''$
γ	$C\,^3\Pi_u$	1	2	4	1		$^{2,4}A'$, $^{2,4}A''$
δ	$E\,^3\Sigma_g^+$	2	1	4	0	1	$^2A'$, $^4A'$
ϵ	$b'\,^1\Sigma_u^+$	2	2	3	1		$^2A'$
Exchange	N_2^+ excitation						
α'	$C\,^2\Sigma_u^+$	2	1	3	1		$^2A'$
		1	2	4	0		
β'	$B\,^2\Sigma_u^+$	1	2	4	0		$^2A'$
		2	1	3	1		
γ'	$A\,^2\Pi_u$	2	2	3	0		$^2A'$, $^2A''$
δ'	$X\,^2\Sigma_g^+$	2	1	4	0		$^2A'$
ϵ'	$^2\Pi_u$ (Ref. 27)	1	1	4	1		$^2A'$, $^2A''$
	$^2\phi_g$ (Ref. 26)	2	2	2	1		$^2A'$, $^2A''$
		2	1	3	1		
		2	2	3	1	$(2\sigma_g)^{-1}$	
ψ'	$^2\Pi_g$ (Ref. 27)	2	2	2	1		$^2A'$, $^2A''$
	He excitation						
κ'	$He^*(1snl) + N_2^+(X)$						
	$He(1s^2) + N_2^{+*}(R)$						
χ'	$He^*(1snl) + N_2^{+*}(R)$						

(b) $He^+ - O_2$

Observed process Direct	O_2 excitation	Electronic configuration $(2\sigma_u)$	$(3\sigma_g)$	$(1\pi_u)$	$(1\pi_g)$	$(n\Lambda)$	$(He-O_2)^+$ Quasimolecular symmetry
X	$X\,^3\Sigma_g^-$	2	2	4	2		$^{2,4}A''$
α	$a\,^1\Delta_g$	2	2	4	2		$^2A'$, $^2A''$
β	$b\,^1\Sigma_g^+$	2	2	4	2		$^2A'$
γ	$A\,^3\Sigma_u^+$	2	2	3	3		$^{2,4}A'$
	$C\,^3\Delta_u$	2	2	3	3		$^{2,4}A'$, $^{2,4}A''$
	$C\,^1\Sigma_u^-$	2	2	3	3		$^2A''$
δ	$B\,^3\Sigma_u^-$	2	2	3	3		$^{2,4}A''$
	$^3\Pi_g(V)$	2	1	4	3		$^{2,4}A'$, $^{2,4}A''$
	$^3\Pi_g(R)$	2	2	4	1	$(3s\sigma_g)$	$^{2,4}A'$, $^{2,4}A''$

TABLE II. (*Continued*).

Observed process Direct	O_2 excitation	(b) $He^+ - O_2$ Electronic configuration $(2\sigma_u)$	$(3\sigma_g)$	$(1\pi_u)$	$(1\pi_g)$	$(n\Lambda)$	$(He - O_2)^+$ Quasimolecular symmetry
Exchange	O_2^+ excitation						
α'	$c\,^4\Sigma_u^-$	1	2	4	2		$^4A''$
β'	$B\,^2\Sigma_g^-$	2	1	4	2		$^2A''$
γ'	$b\,^4\Sigma_g^-$	2	1	4	2		$^4A''$
δ'	$A\,^2\Pi_u$, $a\,^4\Pi_u$	2	2	3	2		$^{2,4}A'$, $^{2,4}A''$
ϕ'	$X\,^2\Pi_g$	2	2	4	1		$^2A'$, $^2A''$
ϵ'	$^2\Sigma_u^-$ (Ref. 32)	2	1	3	3		$^2A''$
		1	2	4	2		
	He excitation						
κ'	$\begin{cases} He^*(1snl) + O_2^+(X) \\ He(1s^2) + O_2^{+*}(R) \end{cases}$						
χ'	$He^*(1snl) + O_2^{+*}(R)$						

sion velocity. The plot as a function of $1/v$ of the probabilities for the exothermic charge-exchange process β', in the He^+-O_2 and He^+-N_2 systems, shown in Fig. 18 is actually consistent with the prediction of the Demkov model. However, the above formula is expected to only provide an upperbound estimate of the transition probability in ion-molecule charge-exchange processes. This is indeed the case for the β' process where the Demkov formula overestimates the experimental results by a factor of $5 \rightarrow 10$. In order to reach better quantitative agreement with experiment, a model is required which properly takes into account averages over the various orientations of the molecule about the intermolecular line. As for the more exothermic charge-exchange processes γ', δ', ϕ', especially, those lying 9 or 12 eV below the incident channel, a direct transition as invoked for process β' is unlikely [predictions based on formula (2) yield results orders of magnitude smaller than the actual findings]. A similar case has already been found in the He^+-Ar system[18(c)] where more complicated mechanisms had to be invoked.

C. Endothermic processes: Curve-crossing mechanisms

The analogy with He^+-Ar and more generally He^+–rare-gas systems can be pushed further. The common characteristics of the currently investigated systems and He^+-RG systems are, as pointed out above, the initial inner $1s$ He vacancy which gives rise to core-excited repulsive states of the triatomic quasimolecule. This feature causes the occurrence of diabatic II (D II) curve crossings[34] between configurations differing by two orbitals namely, $(a'_{1s\,He}\phi\chi)$ and $(a'^2_{1s\,He}\psi)$ around intermolecular distances where the orbital energies satisfy

$$\epsilon_\psi + \epsilon_{1s\,He} = \epsilon_\phi + \epsilon_\chi .$$

Such curve crossings are displayed in the tentative state correlation diagram presented in Fig. 19. The discussed two-electron transition being induced by the $1/r_{12}$ operator, it necessarily involves states of the triatomic molecule having the same symmetry (spatial and spin symmetries). A prototype of such a transition has already been discussed in connection with the population of the $N_2^+(C\,^2\Sigma_u^+)$ state. Note, however, that in this case the curve crossing occurs at large R.

Generally such D II processes populate $[He(1s^2) + M_2^{+*}]$ charge-exchange channels. The excited electron in M_2^{+*} can be either an excited valence or a Rydberg electron. As in the $(He\text{-}Ar)^+$ case, the limit of such excitation series $[He(1s^2) + M_2^{2+}]$ turns out to approximately match the $[He^+(1s) + M_2^+]$ limit: It is thus expected that the energy levels of $[He(1s^2) + M_2^{+*}]$, $[He^*(1s,nl) + M_2^+]$, and $[He^+(1s) + M_2^*]$ series overlap (Fig. 19). Proceeding along the same lines as in the $(He\text{-}Ar)^+$ system, the initially populated $[He(1s^2) + M_2^{+*}]$ channels (D II mechanism) are expected to mediate the observed direct $[He^+(1s) + M_2^*]$ and charge exchange $[He^*(1snl) + M_2^+]$ channels. The actual

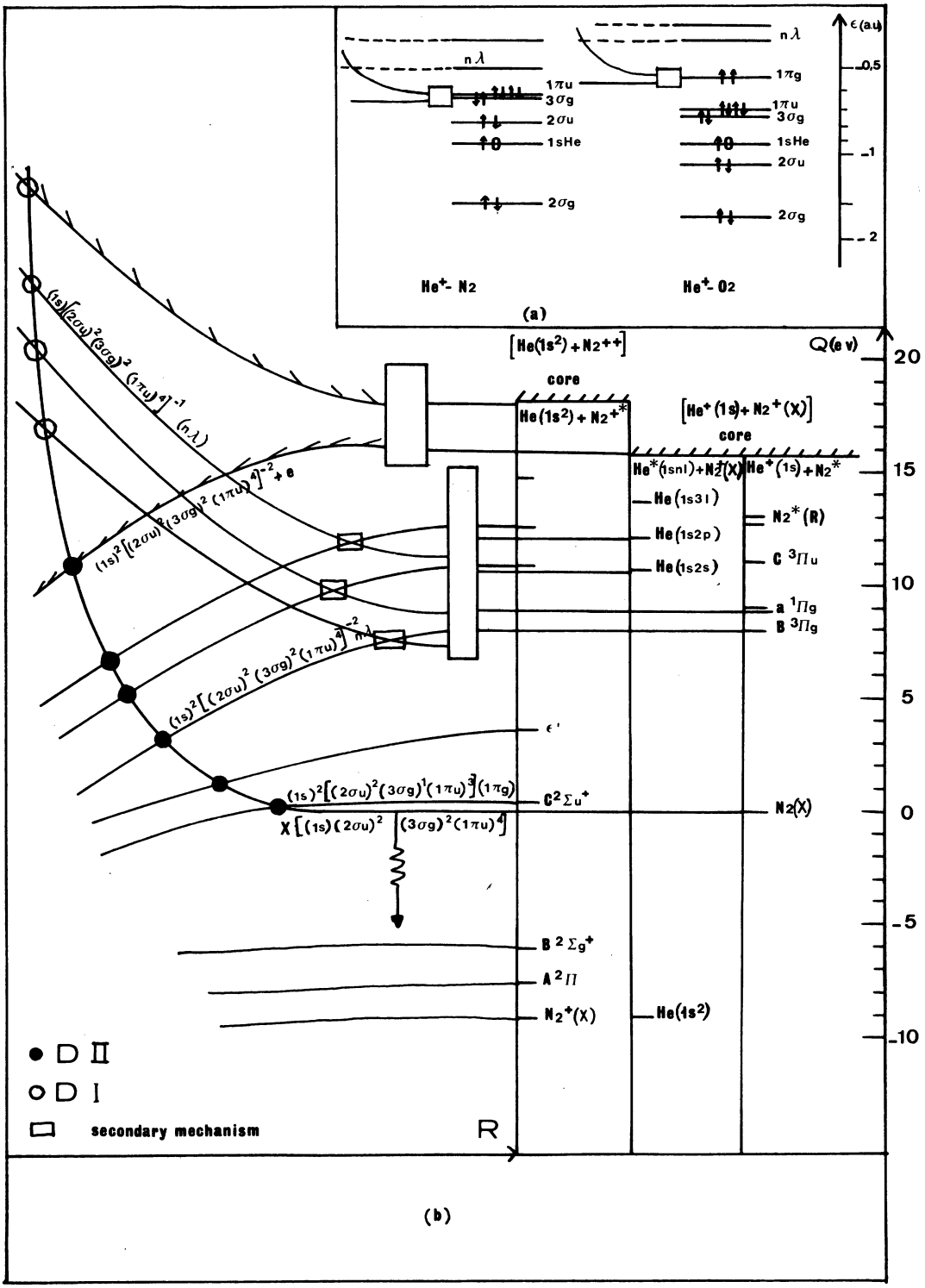

FIG. 19. (a) The relative position of the molecular orbitals of M_2 and the atomic orbital 1s He are displayed together with empty Rydberg MO. The schematic diagram shows the possibility of the occurrence of diabatic II (Ref. 34) (DII) and diabatic I (Ref. 34) (DI) molecular curve crossings. (b) A qualitative molecular-states diagram is proposed. Four types of transitions are symbolized. (i) ⇶ : Direct transition at large intermolecular distance R, (ii) ●: Transitions occurring at a DII curve crossing, (iii) □: one- or two-electron transitions—secondary mechanisms, and (iv) ○: transition occurring at a DI curve crossing.

observation of $[He(1s^2)+M_2^{+*}]$ channels, e.g., ϵ' and ϕ' in N_2 and ϵ' in O_2 supports the suggested D II primary transition. The following scheme illustrates a possible two-step mechanism involving a primary D II transition and yielding process α:

$$He^+(1s)+N_2(X\,^1\Sigma_g^+)$$
$$\downarrow (1)$$
$$a_{1s}'^2 a_{2\sigma_u}'^2 a_{1\pi_u}''^2 (a_{3\sigma_g}'^2\, a_{1\pi_u}'^2)^{-2} a_{1\pi_g}' \rightarrow He(1s^2)+N_2^{+*} \quad (\epsilon')$$
$$\downarrow (2)$$
$$a_{1s}' a_{2\sigma_u}'^2 a_{1\pi_u}''^2\, a_{3\sigma_g}' a_{1\pi_u}'^2 a_{1\pi_g}' \rightarrow He^+(1s)+N_2(B\,^3\Pi_g), \ (\alpha)$$

where the processes indicate (1) primary D II and (2) secondary mechanisms. Since the excitation of $B\,^3\Pi_g$ state satisfies the FC prediction, the above step necessarily occurs in a small intermolecular range, such that during the entire two-step process the nuclei do not move significantly.

Although the above example is given for the He^+-N_2 system, the proposed mechanism should also apply to the He^+-O_2 case. However, in this system, processes α and β require a particular discussion. Since channel α ($O_2\,a\,^1\Delta_g$ state), has 1-eV energy defect with respect to the incident channel X, a direct $^2A''X \rightarrow {}^2A''\alpha$ transition is not *a priori* excluded. This transition involves a two-electron rearrangement and the corresponding interaction, proportional to

$$\left(a_{1s\,He}' a_{1\pi_{gx}}' \left|\frac{1}{r_{12}}\right| a_{1s\,He}' a_{1\pi_{gx}}'\right) + \left(a_{1s\,He}' a_{1\pi_{gy}}'' \left|\frac{1}{r_{12}}\right| a_{1s\,He}' a_{1\pi_{gy}}''\right),$$

decreases exponentially at large intermolecular distances. Consequently, such a transition can be subjected to the Demkov-type model (discussed in Sec. V B). Process β $[He^+(1s)+O_2(b\,^1\Sigma_g^+)\,{}^2A'$ channel] provides a nice example of an A''-A' transition which necessarily requires a rotational coupling (induced by rotation of the triatomic molecular plane). This transition cannot occur directly from the incident channel since the relevant configurations differ by two orbitals. However, one can invoke a multistep mechanism as shown below:

$$A''[He^+ + O_2(X\,^3\Sigma_g^-)] \overset{(1)}{\rightarrow} A''[He^+ + O_2(a\,^1\Delta_g)]$$
$$\overset{(2)}{\rightarrow} A'[He^+ + O_2(a\,^1\Delta_g)]$$
$$\overset{(3)}{\rightarrow} A'[He^+ + O_2(b\,^1\Sigma_g^+)],$$

where the processes indicate (1) "radial" coupling: direct of D II mechanism, (2) rotational coupling, and (3) radial coupling.

The invoked D II mechanism can provide possible explanations of the broad structures observed at energy losses higher than $Q=15.6$ eV ($Q=12$ eV) in the direct-excitation spectra, and $Q=18.1$ eV ($Q=12$ eV) in the charge-exchange spectra of N_2 (O_2). Indeed of the two electrons that participate in the D II process the outermost one can go into a continuum orbital as a natural limit of a Rydberg orbital. Such an explanation has already been found to account for ionization tails in the He^+-RG systems.

Furthermore, the electron filling the $1s$ He vacancy in the D II mechanism can originate from a valence orbital which is not the outermost orbital. In this case, the D II mechanism gives rise to $[He(1s^2)+M_2^{+**}]$ series converging to the excited $[He(1s^2)+M_2^{2+*}+e]$ limit. This new series can then feed $[He^+(1s)+M_2^{**}]$ and $(He^*+M_2^{+*})$ channels, which converge to $[He^+(1s)+M_2^{+*}]$ and $(He^*+M_2^{2+})$, respectively, see Fig. 22. Referring again to the He^+-RG systems it is known that at keV energies the D II processes should strongly decrease, whereas processes induced at D I molecular curve crossings show up. [D I processes result from one- or two-electron transitions at crossings between an initially occupied and promoted molecular orbital (MO) with empty MO's[34]]. These D I processes which are known to become important in violent encounters are likely to account for the behavior as a function of energy of, e.g., κ' and χ' processes (Fig. 11).

VI. CONCLUSION

In this paper, we have reported extensive measurements of both direct and exchange channels in ion-molecule collisions in the medium-energy range. The resolution reached in our experiments has allowed a satisfactory identification of the most important channels. The reported data as a function of collision energy and scattering angle complement and extend previous investigations.

These results show that charge exchange is by far the most important process. Although the near resonant charge-exchange process dominates at low τ, other endothermic channels including $(He^*+M_2^+)$ and $(He+M_2^{**})$ channels show up and compete in more violent collisions, whereas exothermic channels remain weakly excited. These features seem actually to be common to a large variety of He^+-diatom collisions as it will be shown for CO and NO in a forthcoming publication. Beyond the identification of direct-excitation channels high-resolution data enable the investigation of vibrational excitation of the ground state and some electronic states: Work is under way to extend this study as a function of scattering angle.

An interesting outcome of the present results is that several pieces of information prove the cogency of the FC principle within the explored experimental range. According to our classification in Sec. I, the present results illustrate cases of applicability of what we have called the *extended elastic approximation*. Extension of the energy and angular ranges to explore more violent (smaller impact parameter) collisions while maintaining the resolution should allow further investigation of cases entering into the *extended pseudoelastic approximation*. The similarities between the characteristics of the presently investigated systems and the He^+-RG systems has provided the guide line for a tentative interpretation of the mechanisms governing the observed processes. Most interesting is the fact that the majority of the observed processes can be interpreted using either Demkov-type transitions (exothermic processes) or primary D II transition mechanisms followed by secondary population sharings (endothermic processes). The determinant role of the 1s vacancy in these mechanisms can be put to the test by studying neutral He-M_2 collisions.

It is worth stressing that unambiguous interpretation of the spectra requires more molecular data in particular for highly excited neutral and ionic states of diatomic molecules; conversely, the present collision spectroscopy can help in the identification of new molecular states. The validity of the FC principle together with the striking similarity with the He^+-RG systems should simplify the theoretical approach and enable quantitative comparisons.

ACKNOWLEDGMENTS

We are indebted to Professor F. Linder for having provided us with the double hemispherical energy selector and gratefully acknowledge the help of Dr. J. Krutein during the early stages of the building of the apparatus. Thanks are also due to them for valuable discussions and advice.

---

*Present address: also at Centre de Mécanique Ondulatoire Appliquée, 23 rue du Maroc, 75019, Paris, France.

[1]F. T. Smith, R. P. Marchi, W. Aberth, D. C. Lorentz, and O. Heinz, Phys. Rev. 161, 31 (1967).

[2]J. Los, in *Proceedings of the Tenth International Conference of the Physics of Electronic and Atomic Collisions, Paris, 1977*, edited by G. Watel (North-Holland, Amsterdam, 1978), p. 617; J. Los and A. W. Kleyn, in *Alkali Halide Vapors*, edited by P. Davidovits and D. L. Mc Fadden (Academic, New York, 1979) p. 275 and references therein.

[3](a) J. Krutein and F. Linder, J. Phys. B 10, 1363 (1977); (b) J. Krutein and F. Linder, J. Chem. Phys. 71, 599 (1979); (c) F. Linder, in *Electronic and Atomic Collisions*, edited by N. Oda and K. Takayanagi (North-Holland, Amsterdam, 1980), p. 535; (d) Teloy, in *Electronic and Atomic Collisions*, edited by G. Watel (North-Holland, Amsterdam, 1978), p. 591; (e) M. Faubel and J. P. Toennies, Adv. At. Mol. Phys. 13, 229 (1977).

[4](a) J. H. Moore and J. P. Doering, Phys. Rev. Lett. 23, 564 (1969); (b) F. A. Herrero and J. P. Doering, Phys. Rev. A 5, 702 (1972); (c) N. Kobayashi, Y. Itok, and Y. Kaneko, J. Phys. Soc. Jpn. 46, 208 (1979); 45, 617 (1978).

[5](a) J. Fayeton, A. Pernot, P. Fournier, and M. Barat, J. Phys. (Paris) 32, 743 (1971); (b) N. Andersen, H. Vedder, A. Russek, and E. Pollack, J. Phys. B 11, L493 (1978); (c) S. M. Fernandez, F. J. Eriksen, A. V. Bray, and E. Pollack, Phys. Rev. A 12, 1252 (1975); (d) A. V. Bray, D. S. Newman, and E. Pollack, Phys. Rev. A 15, 2261 (1977); (e) H. Inouye, K. Niurao, and Y. Sato, J. Chem. Phys. 64, 1250 (1976); Y. Sato, K. Niverao, H. Takagi, and H. Inouye, *ibid.* 65, 3952 (1976); (f) Fernandez *et al.*, Phys. Rev. Lett. 27, 230 (1971).

[6]V. I. Gerasimenko and J. D. Oksjuk [Sov. Phys.—JETP 21, 333 (1965)]; Zh. Eksp. Teor. Fiz. 48, 499 (1965) Green (T. A.), Phys. Rev. 1, 1416 (1970).

[7](a) J. Baudon, J. Phys. B 6, 850 (1973); (b) P. Sigmund, Phys. Rev. A 14, 996 (1976); (c) J. Phys. B 11, L145 (1978).

[8](a) J. D. Kelley, G. H. Bearman, H. H. Harris, and J. J. Leventhal, Chem. Phys. Lett. 50, 295 (1977); (b) H. Bregman-Reisler and J. P. Doering, J. Chem. Phys. 62, 3109 (1975); R. C. Isler and R. D. Nathan, Phys. Rev. A 6, 1036 (1972); G. H. Saban and T. F. Moran, J. Chem. Phys. 57, 895 (1972); J. H. Birely and D. A. Johson, *ibid.* 62, 4854 (1975); J. H. Birely, Phys. Rev. A 10, 550 (1974); F. Petty and T. F. Moran, *ibid.* 5, 266 (1972); R. F. Holland and W. B. Maier, J. Chem. Phys. 55, 1299 (1971); G. H. Bearman, J. D. Earl, H. H. Harris, D. B. James, and J. J. Leventhal, Chem. Phys. Lett. 44, 471, 1976; G. H. Bearman and J. J. Leventhal, Phys. Rev. A 17, 80 (1978).

[9](a) J. H. Moore and J. P. Doering, J. Chem. Phys. 52, 1692 (1970); (b) J. H. Moore, Phys. Rev. A 9, 2043 (1974); (c) J. H. Moore, J. Geophys. Res. 77, 5567 (1972); (d) J. H. Moore, J. Chem. Phys. 55, 2760 (1971).

[10]W. L. Hodge, A. L. Goldberger, M. Vedder, and E. Pollack, Phys. Rev. A 16, 2360 (1977), and Refs. 5(a), 5(c), 5(d), and 5(e).

[11]K. T. Gillen and A. W. Kleyn, Chem. Phys. Lett. 72, 509 (1980).

[12]In Fig. 4 of Ref. 5(a) the MPEL ΔE_2 for electronic excitation of N_2^+ into the $C\,^2\Sigma_u^+$ state deviates from the discussed behavior [Eq. (1)]. This anomaly is certainly related to the predissociating nature of the $C\,^2\Sigma_u^+$ state. ΔE_2 is indeed a lower bound of the actual MPEL [smaller slope than predicted by Eq. (1)] since N_2^+ ions subject to dissociation do not contribute to the ELS. (Note that the ΔE_2 curve actually parallels

the binary-model curve and not the elastic-model curve as was incorrectly stated there. The conclusion drawn there should consequently be ignored.)

[13]The electronic transition probability amplitudes are assumed to be weakly dependent upon r; if not, the dependence modifies the discussed rovibrational excitation. Nevertheless, this effect can be taken into account properly before projecting the wave packet.

[14]This nomenclature is proposed to extend the earlier elastic approximation which referred to scattering in the absence of electronic excitation.

[15]This nomenclature is proposed to qualify cases where deviations from the elastic approximation occur. It includes the binary model as a limiting case and extends to electronic excitation.

[16]V. M. Lavrov, M. R. Gochitashvili, V. A. Ankundinev, and B. I. Kikiani, Zh. Eksp. Teor. Fiz. 78, 516 (1980) [Sov. Phys.—JETP 51, 260 (1980)].

[17]T. R. Govers, C. A. van de Runstraat and F. J. de Heer, Chem. Phys. 9, 285 (1975); R. F. Stebbings, A. C. H. Smith, and H. Ehrhardt, J. Chem. Phys. 39, 968 (1963); D. W. Koopman, Phys. Rev. 166, 57 (1968); R. Browning, C. J. Latimer, and H. B. Gilbody, J. Phys. B 2, 534 (1969).

[18](a) J. C. Brenot, J. Pommier, D. Dhuicq, and M. Barat, J. Phys. B 8, 448 (1975); (b) M. Barat, J. C. Brenot, D. Dhuicq, J. Pommier, V. Sidis, R. E. Olson, E. J. Shipsey, and J. C. Browne, *ibid.* 9, 269 (1976); (c) V. Sidis, J. C. Brenot, J. Pommier, M. Barat, O. Bernardini, D. C. Lorents, and F. T. Smith, *ibid.* 10, 2431 (1977).

[19]J. C. Brenot, J. Pommier, D. Dhuicq, and M. Barat, J. Phys. B 8, 448 (1975).

[20]F. R. Gilmore, J. Quant. Spectrosc. Radiat. Transfer 5, 369 (1965).

[21]D. C. Cartwright and T. H. Dunning, J. Phys. B 8, L100 (1975).

[22]J. Geiger and B. Schröder, J. Chem. Phys. 50, 7 (1969).

[23]These valence states are known to interact with the $C^1\pi_u$, $C'^1\Sigma_u^+$, $O^1\pi_u$ Rydberg states lying in the same energy-loss range (Ref. 24).

[24]K. Dressler, Can. J. Phys. 47, 547 (1969).

[25]P. K. Carroll and C. P. Collins, Can. J. Phys. 47, 563 (1969); P. Gürtler, V. Saile, and E. E. Koch, Chem. Phys. Lett. 48, 245 (1977); T. N. Rescaigno, C. F. Bender, B. V. McKoy, and P. W. Langhoff, J. Chem. Phys. 68, 970 (1978).

[26]L. Åsbrink and C. Fridh, Phys. Scr. 9, 338 (1974); K. Siegbahn *et al.*, *ESCA Applied To Free Molecules* (North-Holland, Amsterdam, 1969).

[27]M. F. Herman and K. F. Freed, Chem. Phys. 32, 437 (1978).

[28]M. R. Gochitashvili, V. A. Ankudinov, V. M. Lavrov and B. I. Kikiani (private communication, 1979).

[29]R. P. Saxon and B. Liu, J. Chem. Phys. 67, 5432 (1977).

[30](a) D. C. Cartwright, W. J. Hunt, W. Williams, S. Trajmar, and W. A. Goddard, Phys. Rev. A 8, 2436 (1973); (b) S. Trajmar, D. C. Cartwright, and R. Hall, J. Chem. Phys. 65, 5275 (1976).

[31]O. Edquist, E. Lindholm, L. E. Salin, and L. Asbrink, Phys. Scr. 1, 25 (1970); R. N. Dixon and S. E. Hull, Chem. Phys. Lett. 3, 367 (1969).

[32]N. Honjou, K. Tanaka, K. Ohno, and H. Taketa, Mol. Phys. 35, 1569 (1978).

[33]Y. N. Demkov, Zh. Eksp. Teor. Fiz. 45, 195 (1963) [Sov. Phys.—JETP 18, 138 (1964).

[34]J. C. Brenot, D. Dhuicq, J. P. Gauyacq, J. Pommier, V. Sidis, M. Barat, and E. Pollack, Phys. Rev. A 11, 1245 (1975).